Compensating Parasitic Collisions Using Electromagnetic Lenses

J.-P. Koutchouk, J. Wenninger, F. Zimmermann
CERN, 1211 Geneva 23, Switzerland

Long-range collisions are important not only for e+e- factories, but they also limit the dynamic aperture of hadron colliders. Their effect can be compensated by a current-fed wire mounted parallel to the beam. A compensation scheme based on this idea has been proposed for the Large Hadron Collider (LHC). First, successful machine experiments with a prototype device in the CERN SPS explored the dependence on the beam-wire distance and on the wire excitation. Various different types of beam signals and monitors were used to gather maximum information about the impact of the wire on beam dynamics. Two additional devices will be installed in 2004, in order to explicitly demonstrate the compensation, to study pertinent tolerances, and, furthermore, to assess the respective merits of different beam-beam crossing schemes for several interaction points.

1. MOTIVATION

Long-range beam-beam collisions are unavoidable in colliders with close bunch spacing. Even with a crossing angle at the main collision point, they can perturb the motion at large betatron amplitudes, where particles come close to the opposing beams. The long-range collisions may give rise to a diffusive aperture [1], beyond which particles are lost quickly from the beam, to enhanced background in the particle-physics detector, and to a poor beam lifetime. The effect of the long-range collisions is found to be an increasing problem for successive generations of hadron colliders that is for operation with an ever larger number of bunches, ranging from the CERN Super Proton Synchrotron (SPS), over the FNAL Tevatron, to the Large Hadron Collider (LHC). This is illustrated in Table 1, which lists the number of 'parasitic' long-range encounters at these three colliders.

Table 1: Nominal number of long-range collisions per bunch at various hadron colliders.

	#LR encounters
SPS	9
Tevatron Run-II	70
LHC	120

The LHC features the largest number of long-range collisions of the three colliders in Table 1. Figure 1 displays a schematic layout of the LHC with its 4 main collision points. The parasitic collisions surrounding the primary interaction points (IPs) are illustrated in Fig. 2. In the LHC, there are 30 long-range collisions around each of the four primary IPs, and thus 120 long-range encounters in total. A partial mitigation of the long-range effect can be achieved by exploiting cancellations between the different IPs. For example, by crossing the beams in one IP horizontally and in another vertically, the linear components of the long-range beam-beam force at the two IPs exactly cancel each other [2,3]. However, the nonlinear components of the force do not, in general, compensate each other, but in many cases add. The SPS experiment is capable of 'simulating' a 'worst' case, where the forces experienced at all parasitic collisions around the two main LHC IPs (i.e., at ATLAS and CMS) would add linearly.

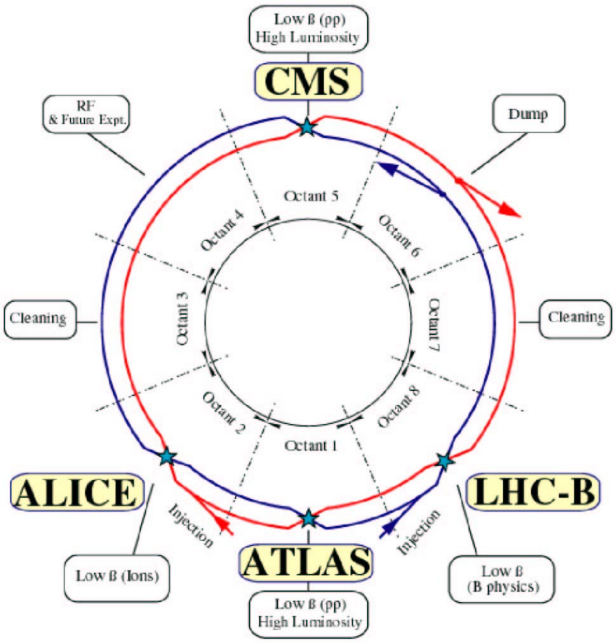

Figure 1: Schematic of the LHC with the two counter-rotating beams and 4 primary collision points.

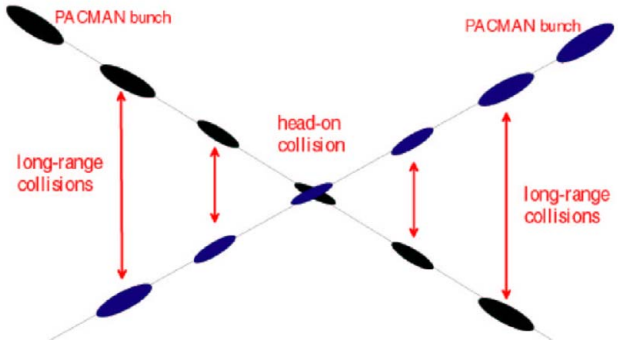

Figure 2: Schematic of long-range encounters around a primary collision point, including PACMAN bunches at the head or tail of a bunch train.

In 1999, simulations by T. Sen et al. indicated that in the LHC particle amplitudes above 7σ grow with time. A sharp threshold was observed for a 300 μrad crossing angle [4]. Y. Papaphilippou and F. Zimmermann noted a

strong diffusion in action (Courant-Snyder invariant) above a certain threshold amplitude, for a simplified 4-D tracking model. Figure 3 shows a typical result [5]. Whenever long-range collisions are present, and independent of the primary head-on collisions, a 'diffusive aperture' exists at start amplitudes of about 5.5-6σ in both transverse planes, if the beams are separated by 9.5σ. In these simulations, the diffusion is computed from a group of particles launched at the same initial amplitude, but with a random betatron phase. The dependence of this 'diffusive aperture' threshold on various parameters was also studied in [5].

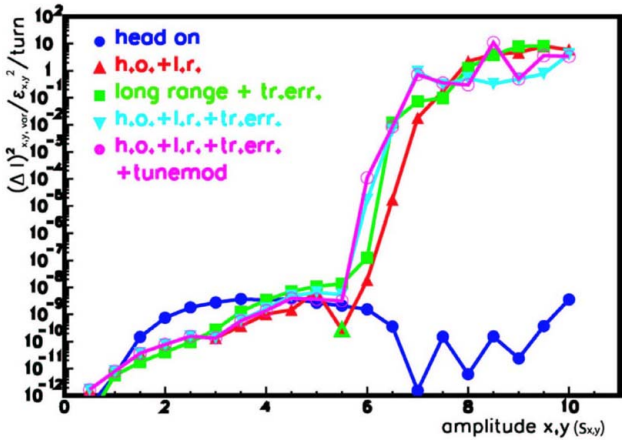

Figure 3: Simulated increase of action variance per turn in units of the nominal design emittance as a function of horizontal and vertical start amplitude in σ for various combinations of head-on collisions, long-range collisions, triplet field errors, and tune modulation [5]. For the blue curve the long-range collisions are absent. The vertical axis is shown on a logarithmic scale.

Performing 6-dim. tracking studies for a complete model of the LHC, F. Schmidt et al. found that the dynamic aperture (defined by particle loss) strongly decreases with an increasing number of turns, if long-range collisions are taken into account [6]. Over 10^6 turns the minimum dynamic aperture is only 6σ, and some chaotic trajectories are found already at 4σ. At injection, despite of a larger separation, F. Schmidt found a dynamic aperture of still only 7σ, again limited by the long-range collisions [7].

2. LONG-RANGE BEAM-BEAM COMPENSATION FOR THE LHC

To correct all nonlinear effects, the compensation must be local. A correction scheme was proposed by J.-P. Koutchouk [8,9]. It consists of a wire running parallel to the beam approximately the same transverse distance in units of rms beam size as the opposing beam at the parasitic collision points. The wire is mounted where the beams are already separated, but the betatron phase still is approximately the same as at the points of the long-range encounters. The proposed location of the long-range compensators in the LHC is 41m downstream of the separation dipoles D2 on both sides of IP1 and IP5 (see Fig. 1) [8], as sketched in Fig. 4. The average difference in betatron phase between the compensator and the associated long-range collisions is 2.6° [8], which, according to simulations, is sufficiently close to zero [10].

How can we scale the LHC situation to the SPS? The deflection of a particle by the wire is

$$\Delta y' = \frac{2 r_p l_w I_w}{\gamma e c (y - d)} \qquad (1)$$

where r_p denotes the classical proton radius, l_w the length of the wire, I_w the wire excitation current, γ the Lorentz factor, y the particle amplitude with respect to the closed orbit, d the separation between the beam center and the wire center, the prime the derivative with respect to longitudinal position, e the proton charge, c the speed of light, and we have assumed a purely vertical separation. An analogous expression applies to the beam-beam long-range collision. In this case the parameter d denotes the distance between the two beam centers, and the integrated wire strength $I_w l_w$ must be replaced by the bunch population N_b and by the number of parasitic collision on one side of the IP n_b according to

$$\frac{I_w l_w}{ec} = N_b n_b \qquad (2)$$

This last equation also determines the wire current that is equivalent to the LHC situation. The scaling becomes evident, if we normalize the deflection by the rms beam divergence. Then we obtain for the relative perturbation

$$\frac{\Delta y'}{\sigma_{y'}} = \left(\frac{2 r_p l_w}{ec} \right) \left(\frac{I_w}{(\gamma\varepsilon)\tilde{n}_{da}} \right) \qquad (3)$$

where on the right-hand side we recognize the integrated strength of the wire ($I_w l_w$), the normalized emittance ($\gamma\varepsilon$), and the amplitude, e.g., at the diffusive aperture, in units of sigma, $\tilde{n}_{da}$. In particular, if the beam-wire (or beam-beam) distance is held constant in units of rms beam size and if the normalized emittance is constant as well, the diffusive aperture in terms of sigma depends neither on the beam energy nor on the beta function.

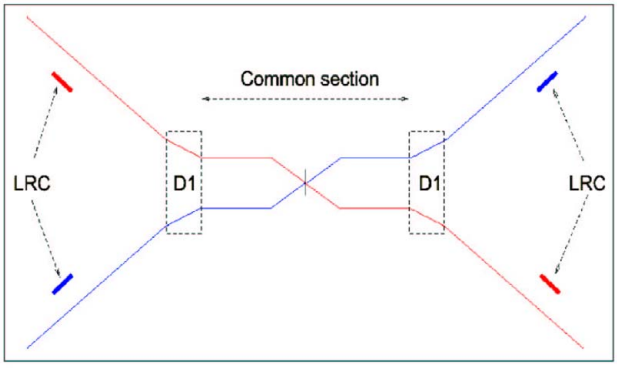

Figure 4: Schematic of the LHC beam-beam compensators mounted on either side of IP1 and IP5 upstream of the separation dipoles.

3. SPS MACHINE EXPERIMENTS

3.1. Prototype Compensator Device

In 2002 two adjacent 60-cm long water-cooled thin (outer and inner diameter 2.54 and 1.54 mm) copper wires were installed in the CERN SPS. The maximum current of 267 A is sufficient to model the accumulated effect of 60 long-range collisions in the LHC, i.e., the total number of long-range collisions around IP1and IP5 (the nominal beam-beam separation is higher at the other two IPs).

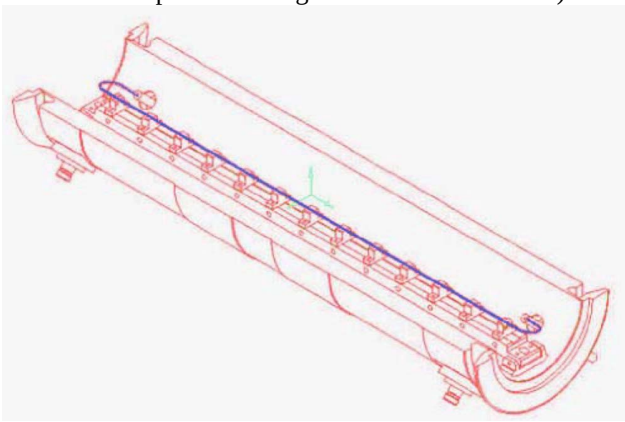

Figure 5: Drawing of 2002-2003 experimental set-up in the SPS showing one of the two 60-cm long wires installed with multiple supports and replacing two of the four original antennas in a beam-position monitor.

The nominal distance between the outer edge of the wire and the centre of the vacuum chamber is 19 mm (Fig. 6), which places the wire in the shadow of the arc-chamber aperture. Figures 7 and 8 display technical drawings of a cross section and a side view for the SPS wire set up.

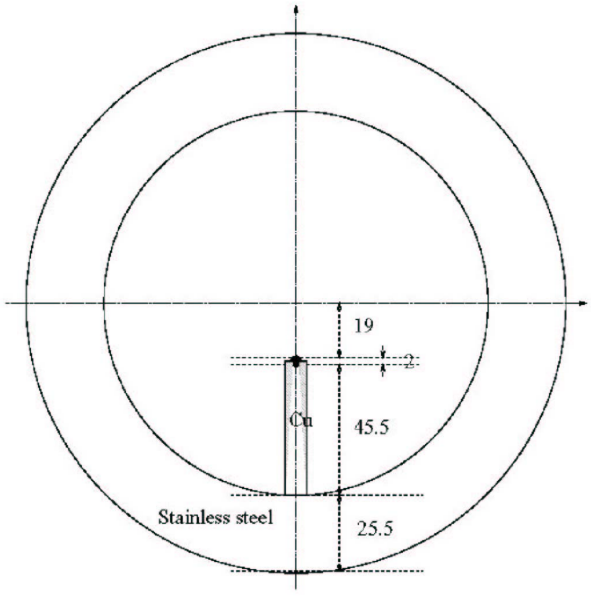

Figure 6: Schematic cross section of the SPS wire with surrounding beam pipe. All numbers are given in units of mm.

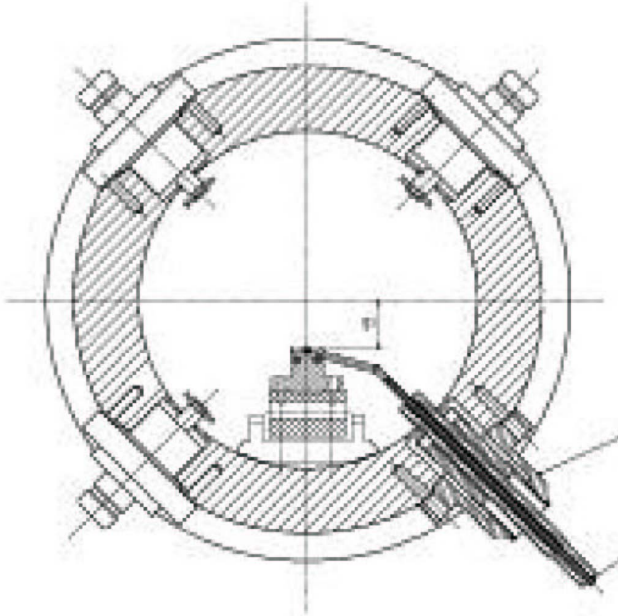

Figure 7: Cross section of beam pipe and wire.

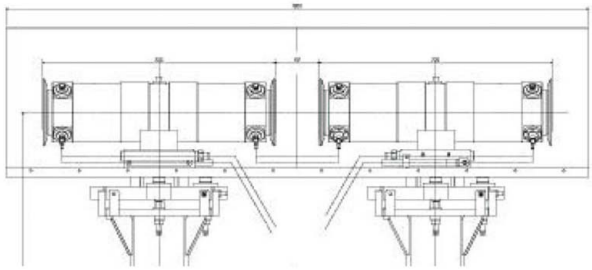

Figure 8: Side view of the two adjacent wires already installed in the SPS, with a total effective length of 1.2 m.

3.2. Simulations

Simulations confirm that the SPS wire and the long-range collisions in the LHC should cause similar fast losses at large amplitudes. As an example, the simulated growth in particle amplitude during 1 second due to the induced diffusion is shown as a function of the starting amplitude in Figs. 9 and 10, for the LHC and the SPS experiment, respectively. The amplitude values on both axes refer to typical locations with a beta function of 80 m or 50 m, for the two accelerators. In more detail, the simulation indicates that the diffusion in the action variable

$$I = \frac{y^2 + (y'\beta + y\alpha)^2}{2\beta} \qquad (4)$$

is chaotic [1,5], and, therefore, we have first computed the action diffusion coefficient

$$D(I) = \frac{1}{2}\frac{<(\Delta I)^2>}{\Delta t} \qquad (5)$$

where the angular brackets denote an average over an ensemble of particles launched at the same nominal action value with radom betatron phases. Since the maximum oscillation amplitude at a location with beta function β is

$$\hat{y} = \sqrt{2\beta I} \qquad (6)$$

the amplitude growth during time Δt was obtained as

$$\Delta\hat{y} = \sqrt{\frac{\beta}{2I}}\Delta I = \sqrt{2D(I)\Delta t}\,\frac{\beta}{\hat{y}} \quad . \qquad (7)$$

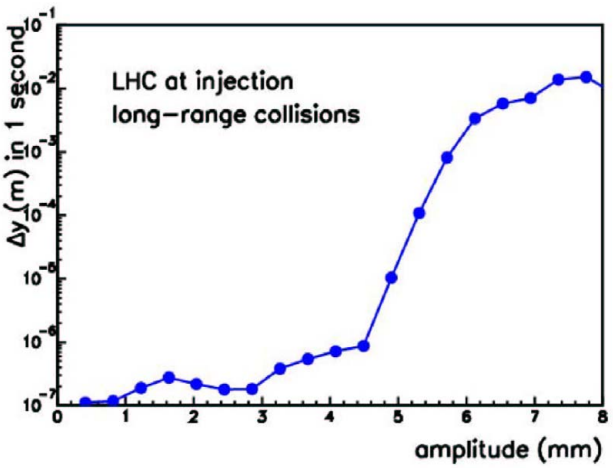

Figure 9: Simulated amplitude growth in mm during 1 second due to long-range beam-beam collisions in the LHC at injection as a function of starting amplitude. The amplitude growth was inferred from the simulated action diffusion coefficient $(\Delta I)^2/\Delta t$ for a typical LHC beta function of β=80 m using (7).

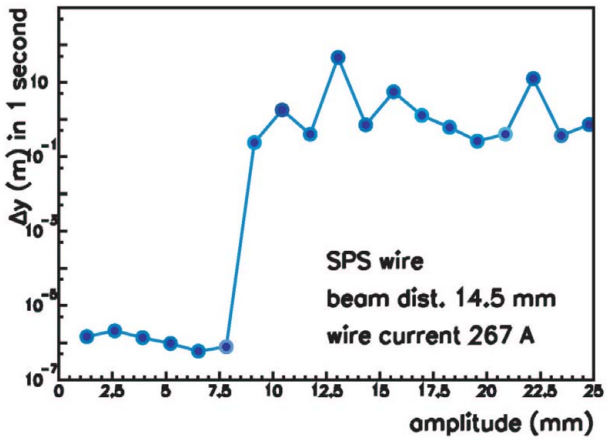

Figure 10: Simulated amplitude growth in mm during 1 second at 55 GeV/c for a 267-A excitation of the SPS wire as a function of starting amplitude. The amplitude growth was inferred from the simulated action diffusion coefficient $(\Delta I)^2/\Delta t$ for the beta function at the wire of β=50 m using (7).

Comparing Figs. 9 and 10, we note that both reveal a 'diffusive' aperture - in one case at about 4.5 mm and in the second case at about 8 mm -, above which the diffusion rate steeply increases. The absolute growth rates outside of the diffusive aperture are also similar, reaching several mm per second in either case.

3.3. Overview of Machine Studies

A total of six machine experiments were performed in 2002 and 2003. Their main features, objectives and accomplishments are summarized as follows:

1) On 20.08.2002 at 26 GeV/c, we recorded the reading of ion chambers and photo-mulipliers versus the beam position at the wire. A clear threshold was observed. The wire excitation was 120 A, limited by wire-current ripple at higher excitation levels. A tune shift of $\Delta Q_{x,y}$=-/+0.0060 was induced by the wire in the two planes.
2) On 10.09.2002 at 26 GeV/c we commissioned a new inductive coil to suppress current oscillations. The wire temperature increased by more than 18 K at 275 A, in agreement with expectation. We attempted to blow up the transverse emittance by 'damper chirps' (with help by W. Hofle). Both tune shift and orbit distortion were recorded as a function of the bump amplitude at the wire for excitation currents of 120 and 267 A.
3) On 23.09.2002 at 55 GeV/c, we again blew up the vertical emittance by the damper. A severe vertical aperture problem was encountered (the physical aperture was much smaller than in previous studies conducted at lower energy, so that the normalized aperture in units of beam sizes was even lower than at 26 GeV/c, defeating the purpose of the increased beam energy). The emittance was observed to shrink due to particle losses for beam-wire distances of less than 12 mm. We recorded beam lifetime and losses as a function of the beam-wire separation.
4) On 27.06.2003 at 26 GeV/c a new dipole was available at the position of the wire, so that the ensuing orbit distortion can be corrected locally. Again particle loss and emittance shrinkage were observed, when the wire was excited.
5) On 04.07.2003 at 26 GeV/c, the emittance was increased by a mismatch in the transfer line. The emittance shrinkage due to particle loss was studied as a function of wire current.
6) On 21.08.2003 at 26 GeV/c, deflecting a small 'pencil beam' by a fast kicker, we took transverse turn-by-turn data at all beam-position monitors over the next 1000 revolutions. Then, for a similar beam as in 5) we re-measured the emittance shrinkage, this time as a function of the beam-wire separation. We calibrated the wire scanner signals by mechanical scraping, and we finally attempted to measure the diffusion rate as a function of amplitude by collimator retraction.

The important results are further detailed below.

3.4. Linear Optics Perturbations

The most direct effects of the wire that can be detected are changes in the linear beam optics, i.e., a closed-orbit

distortion and a change in the two betatron tunes. The shifts in the beam-wire distance d and in the tune Q due to the wire are given by the following two equations:

$$\Delta d = \frac{\beta I_w l_w r_p}{\gamma e c (d+\Delta d)\tan(\pi(Q+\Delta Q))}$$
$$\Delta Q = \pm \frac{r_p I_w l_w}{2\pi\gamma e c}\frac{1}{(d+\Delta d)^2} \quad (8)$$

where I_w denotes the wire current, l_w the wire length, and d the initial beam-wire distance (prior to wire excitation). In principle, the two coupled equations above must be solved together. In practice we found that monitoring either of these two or three (2 tunes) quantities alone provides an accurate and consistent determination of the beam-wire distance with a precision of a few percent. Similar equations would describe the change in orbit and position at the LHC due to the other beam, only that in this case both beams are free to move, while in the SPS experiment the wire position is fixed. The measured changes in the closed-orbit distortion and in the tunes as a function of the beam-wire separation are in excellent agreement with the MAD prediction, as is illustrated in Figs. 11-13.

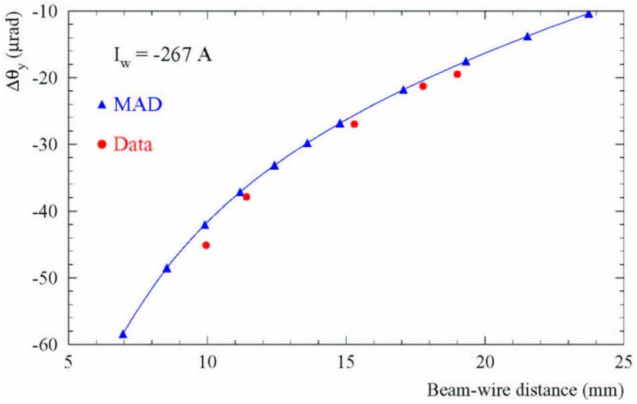

Figure 11: Closed-orbit deflection angle at the wire either fitted from the nearby BPM readings or predicted by MAD as a function of the beam-wire distance for a wire current of 267 A at 55 GeV/c.

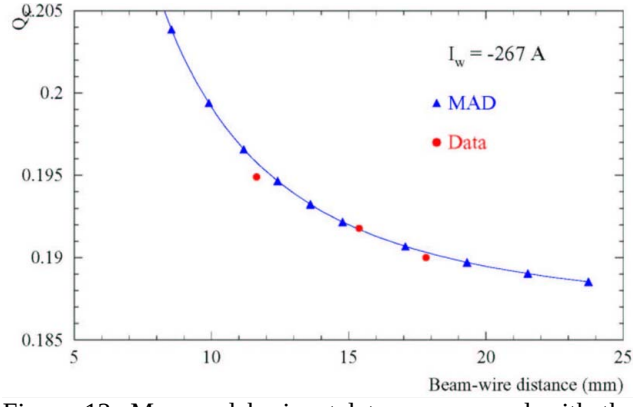

Figure 12: Measured horizontal tune compared with the MAD prediction as a function of the beam-wire distance for a wire current of 267 A at 55 GeV/c

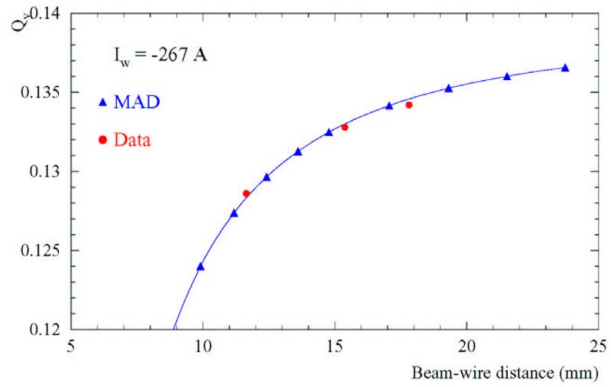

Figure 13: Measured vertical tune compared with the MAD prediction as a function of the beam-wire distance for a wire current of 267 A at 55 GeV/c.

Therefore, the beam-wire distance after wire excitation can be inferred from either the tune shift or the orbit change. Example results are plotted in Fig. 14, together with the analytical prediction, as a function of the initial distance for zero wire current.

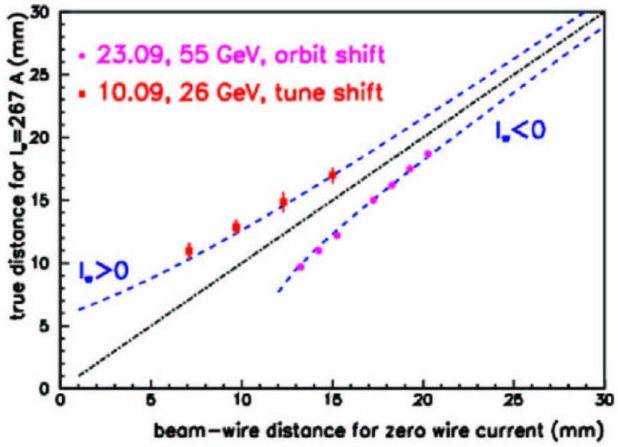

Figure 14: Actual distance between beam and wire when the wire is excited at 267 A as a function of the initial beam-wire separation without excitation. The upper plotting symbols show distances inferred from the measured tune shift for positive wire current at 55 GeV/c via the first Eq. (8). The lower plotting symbols are distances inferred) from the measured orbit change for negative wire current at 26 GeV/c using the second Eq. (8). The two dashed blue lines represent the theoretical prediction (8) based on the known step size along the horizontal axis. For the 26 GeV data the zero of the horizontal axis was adjusted such that the right-most point coincided with the prediction. For the 55 GeV/c case no such adjustment was made; instead the horizontal zero point was extrapolated from the orbit readings and the known position of the wire.

3.5. Diffusive Aperture

The third machine development (MD) study of 2002 yielded evidence for a threshold in the beam lifetime as a function of the beam-wire separation. This is shown in

Fig. 15. When the wire was excited, we observed a steep drop in the beam lifetime, for a beam-wire separation smaller than about 9σ. For 7-8σ separation, the beam lifetime decreased to about 1-5 h due to the wire. We also directly monitored the beam loss by a series of photomultipliers mounted in the vicinity of the beam pipe at strategic locations. If the wire is excited, the beam loss signal, displayed in Fig. 16, exhibits the same sharp threshold as the beam lifetime.

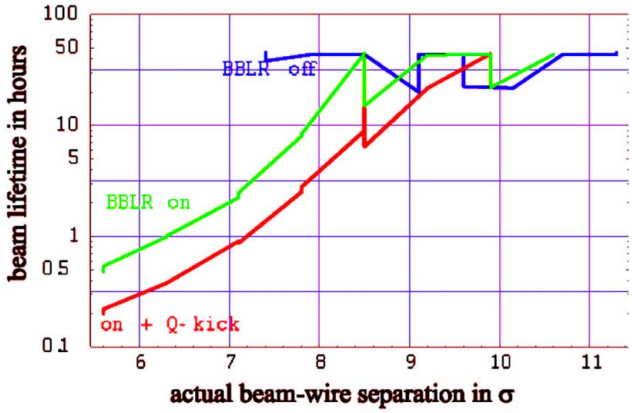

Figure 15: Beam lifetime as a function of beam-wire separation at 55 GeV/c. The three curves refer to the cases without wire excitation (blue top curve – no drop in the lifetime!), with the wire excited (green center curve), and with wire excited and tune kicker active (red bottom curve).

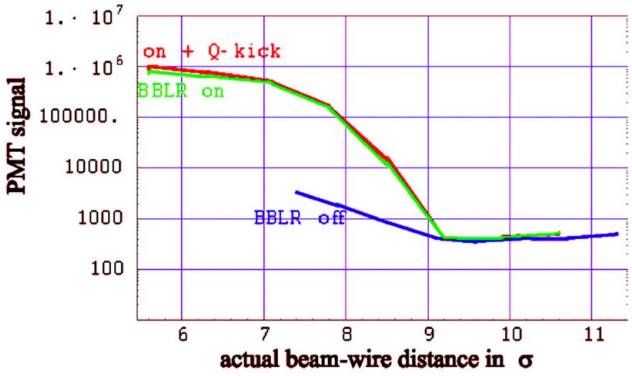

Figure 16: Beam loss signal detected by a photomuliplier as a function of the beam-wire separation for the same three cases as in Fig. 15.

The measurements displayed in Figs. 15 and 16 are reminiscent of the variation in the diffusion rate as a function of crossing angle simulated for the LHC [5], e.g., the diffusion at 5σ is reproduced in Fig. 17. It shows a sharp threshold near a beam-beam separation of about 9σ similar to that seen in the SPS experiment.

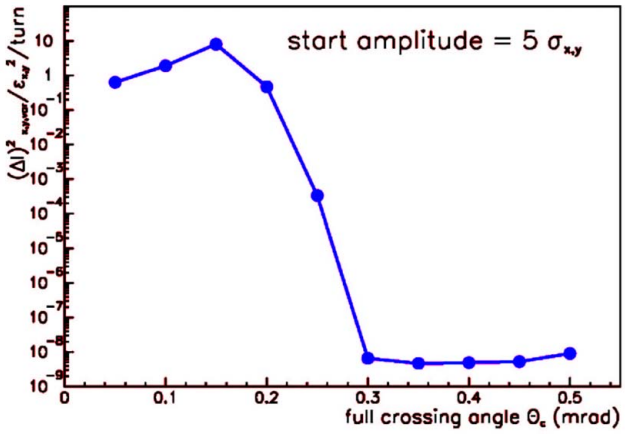

Figure 17: Simulated diffusion rate in LHC (action variance increase per turn in units of the square of the nominal emittance) as a function of the crossing angle [5].

Figure 18 shows the reduction in the final beam emittance due to particle loss, if the wire is excited. In the limit of large initial emittances, the final emittance seems to approach a constant value. The beam shrinks, since the particles at large amplitudes are lost. From the measured asymptotic emittances and associated wire scans we can infer the 'diffusive aperture'.

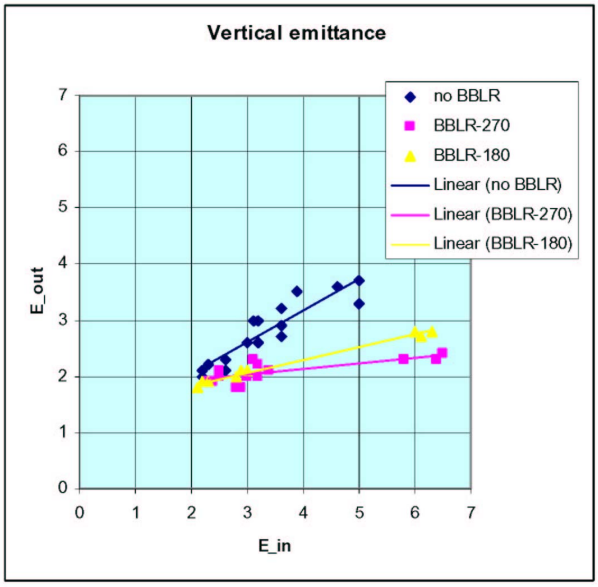

Figure 18: Final vertical emittance after wire excitation as a function of initial emittance. The three data sets refer to three different wire currents: 0 A (blue, top), 180 A (yellow, centre), and 270 A (pink, bottom).

In Fig. 19, its measured values are shown as a function of the square root of the wire current and compared with both the simulation and a scaling law proposed by Irwin [1].

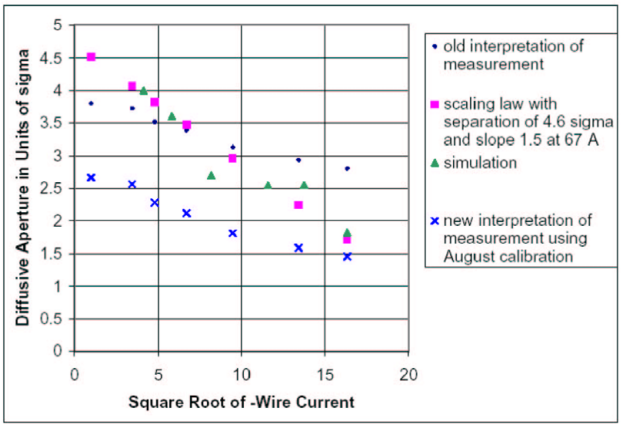

Figure 19: Diffusive aperture as a function of wire current. The small blue dots show an old interpretation of the measured data, the blue crosses (bottom) a revised interpretation, that was obtained from a calibration of the wire scan by a mechanical scraper, the pink squares indicate a straight line representing Irwin's scaling law with estimated intercept and slope, and the green circles are simulation results.

The measurement shows the expected linear dependence on the square root of the wire current, but the inferred aperture values are smaller than expected from the simulations. This could either imply that the simulation is optimistic or it could hint at an error in the interpretation of the wire scans in terms of aperture.

Figure 20 presents the final emittance after wire excitation and in particular its dependence on the beam-wire separation. The latter was varied by an orbit bump. Results are shown for three different wire currents. Multiple values in the vertical direction indicate the variation caused by tune changes.

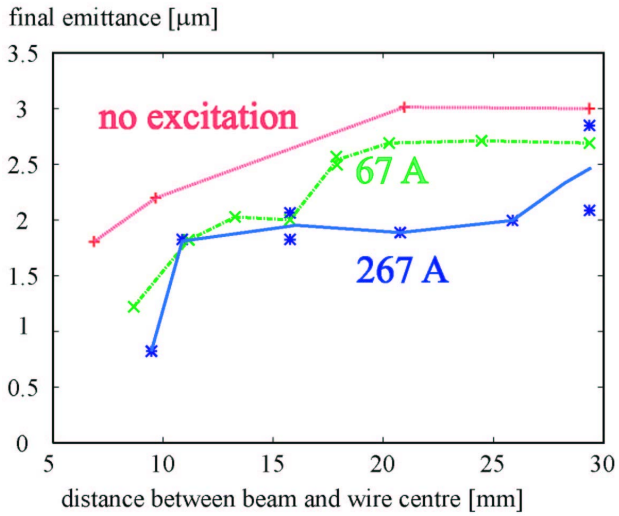

Figure 20: Final normalized emittance versus the distance between wire-centre and beam at 26 GeV/c. The three curves correspond to wire currents of 0, 67 and 267 A.

For the left outermost point without wire excitation, the reduction in emittance would be consistent with mechanical scraping at an amplitude of (6.87-1.27) mm = 5.6 mm (where 1.27 mm is the wire radius), corresponding to the distance from the edge of the wire. As shown in Fig. 20, this value also roughly equals the dynamic aperture for a 267-A wire excitation at the nominal distance 20.27 mm.

Wire scans were performed at 100 ms (IN scan) and after 3200 ms (OUT scan) in the same SPS cycle. Wire excitation or mechanical scraping started at 1500 ms. Figure 21 shows the IN and OUT scans without wire excitations, when the beam was mechanically scraped at an amplitude of +3.06(+0.88)mm, which gave a final normalized rms emittance of 1.7 μm (the additional 0.88 mm are a fitted offset of the scraper position). Bumping the beam to –11.6 mm for a wire excitation of 67 A yielded a roughly comparable emittance of 2.2 μm. The associated wire scans are displayed in Fig. 22. Finally, for the larger wire current of 267 A already a reduced bump of –9.4 mm resulted in an emittance as small 1.15 μm, as illustrated by the wire scans in Fig. 23.

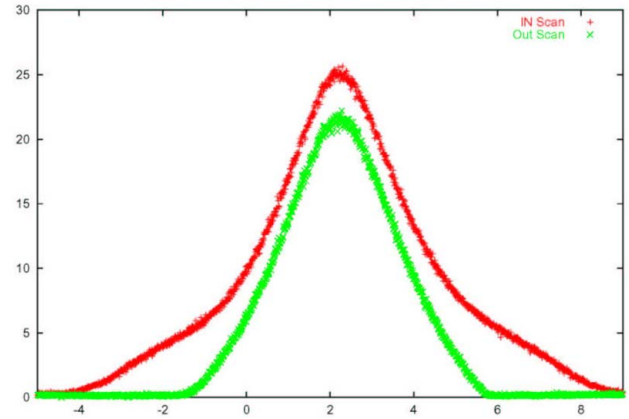

Figure 21: Wire scans before and after mechanically scraping at 3.94 mm from the beam center.

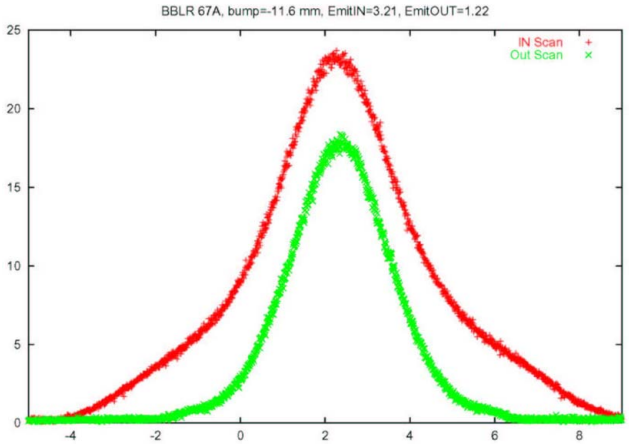

Figure 22: IN and OUT wire scans for a bump amplitude of –11.6 mm and a wire current of 67 A.

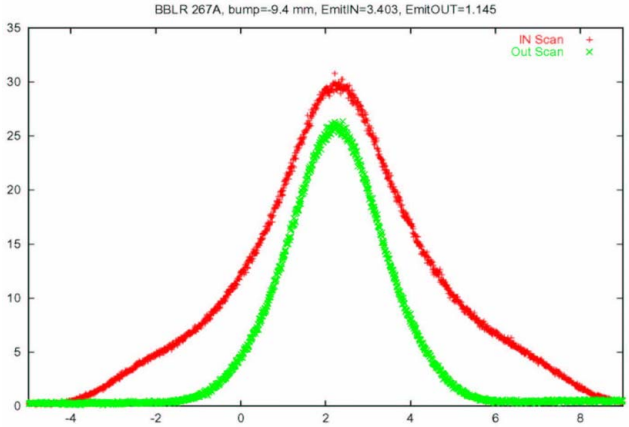

Figure 23: IN and OUT wire scans for a bump amplitude of –9.4 mm and a wire current of 267 A.

To extract the dynamic or diffusive aperture from the IN and OUT wire scans it is sensible to first convert the wire scans into action or amplitude space, which - for a symmetric beam and profile - can be done by an Abel transformation of the form [11,12,13]

$$\rho(A) = -2A\int_{A}^{R} d\eta \frac{g'(\eta)}{\sqrt{\eta^2 - A^2}}$$

where A denotes the normalized amplitude, η the normalized wire-scan coordinate [12], $g(\eta)$ is the measured profile, and $g'(\eta)$ its derivative, and R is an outer limit, e.g., corresponding to the limiting range of the wire scan.

Figures 24 and 25 show amplitude distributions computed from the IN and OUT scans performed before and after mechanically scraping at 3.06(+0.88) mm and 2.06(+0.88) mm from the beam centre, as well as the difference distribution. The associated final emittances are 1.71 μm and 1.31 μm. Figures 26 and 27 present similar distributions obtained for a excitation at 267 A. They correspond to final emittances of 2.06 μm and 1.15 μm.

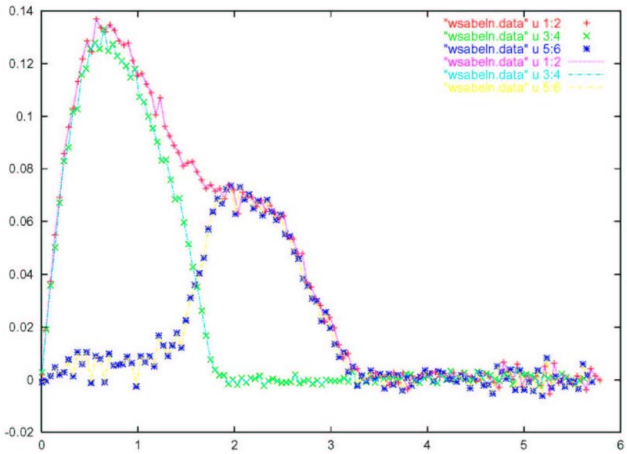

Figure 24: Amplitude distributions for IN and OUT scans with mechanical scraping at 3.06(+0.88)mm, and their difference, as a function of the normalized amplitude in units of σ for ε_N=3.75 μm.

The difference distributions shown in Figs. 24-27 represent the 'lost' or 'scraped' parts of the distribution. They should be positive definite, as nearly fulfilled in the above examples. However, in some other cases these distributions assume large negative values. Possible reasons are under investigation.

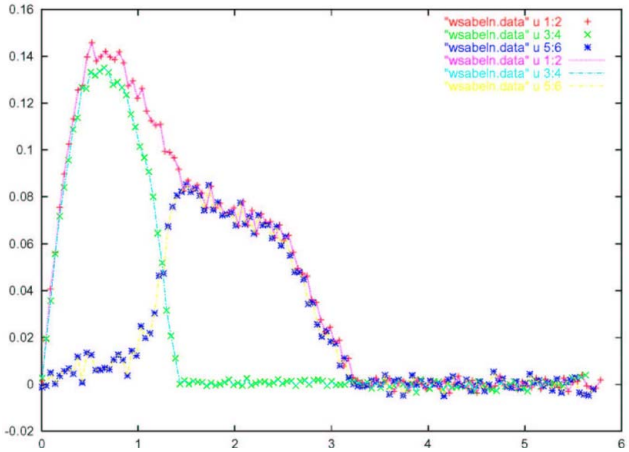

Figure 25: Amplitude distributions for IN and OUT scans with mechanical scraping at 2.06(+0.88)mm, and their difference, as a function of the normalized amplitude in units of σ for ε_N=3.75 μm.

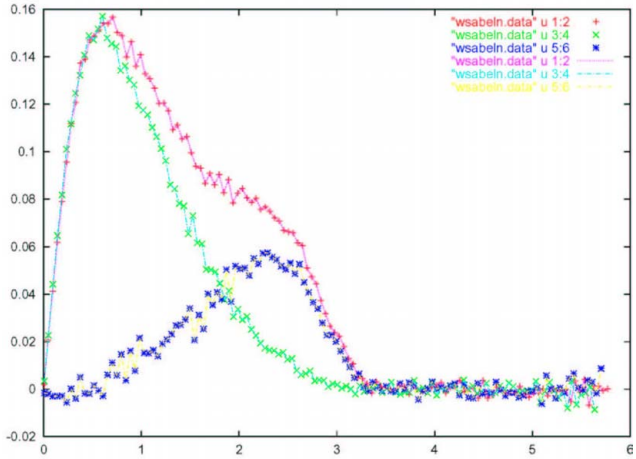

Figure 26: Amplitude distributions for IN and OUT scans with267 A wire excitation and a bump of –4.5 mm, and their difference, as a function of the normalized amplitude in units of σ for ε_N=3.75 μm.

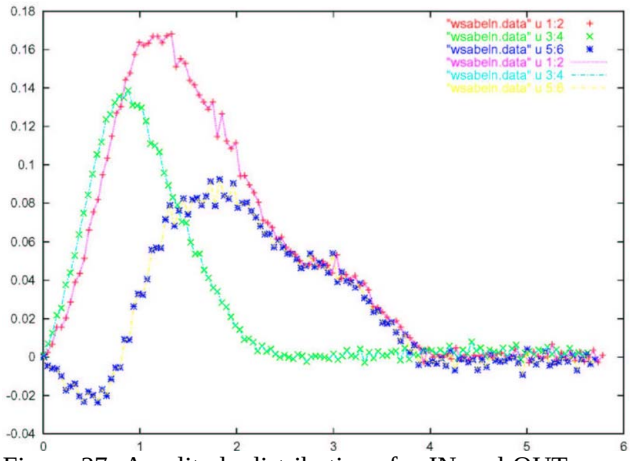

Figure 27: Amplitude distributions for IN and OUT scans with267 A wire excitation and a bump of –9.4 mm and their difference, as a function of the normalized amplitude in units of σ for ε_N=3.75 μm.

The calibration curve in Fig. 28 shows the final emittance as a function of the scraper position. This curve is almost perfectly parameterized by a linear fit (which may suggest that the transverse distribution is not a Gaussian). It allows us to estimate the effective 'diffusive' aperture due to the wire excitation from wire- scan emittance measurements. Using this calibration, we can scale the data of Fig. 20 to the LHC, which gives the curves in Fig. 29. The decrease in aperture for small crossing angles is real, but the maximum values on the right might be underestimated due to the limited mechanical aperture of the SPS at 26 GeV/c.

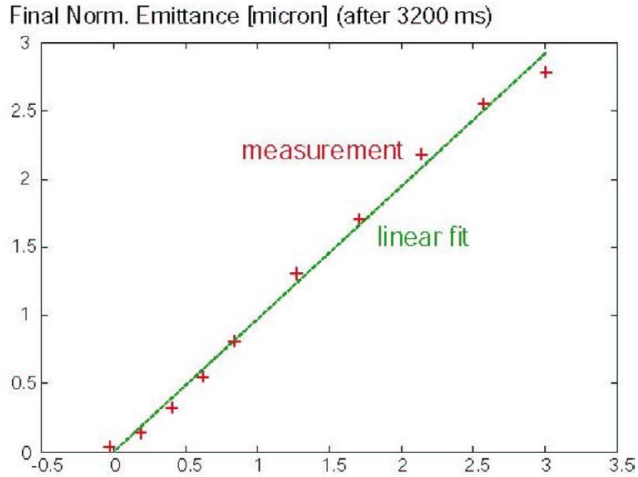

Figure 28: Final emittance as a function of the position of the mechanical scraper in units of the SPS rms beam size (2.3 mm for an emittance of 3.25 μm), corrected by an offset of 0.88 mm.

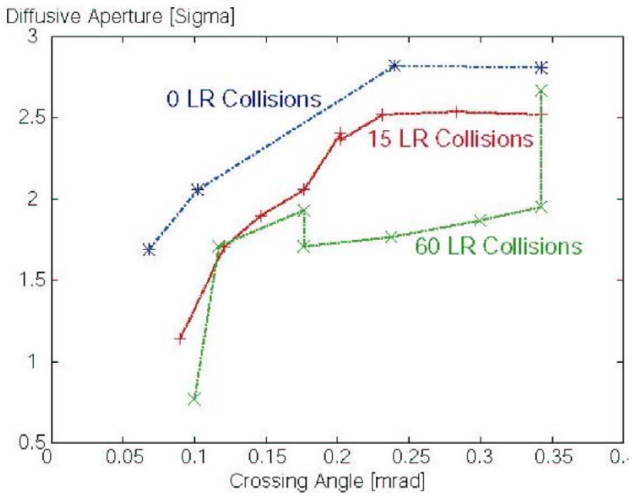

Figure 29: SPS data of Fig. 20 converted to the LHC situation: diffusive aperture vs. crossing angle for three different numbers of long-range collisions.

Figures 30 and 31 show typical beam loss signals during the SPS cycle in the presence of wire excitation and mechanical scraping. In particular, the second figure, 31, illustrates the attempt of a diffusion measurement. The PMT and wire being just downstream of the scraper, the PMT signal also detects the debris from the scraping at about 13325 ms. From the reduction of the signal after the scraping and the subsequent slow recovery one can extract a diffusion coefficient [14]. In Fig. 31, the scraper approaches the beam through about 1σ. At larger amplitudes the diffusion appears to be much faster than the speed of the scraper (as expected), and, for this reason among others, it has not yet been possible to accomplish a reliable and clear diffusion measurement at these larger amplitudes. Note that in Fig. 31, a nonzero beam-loss signal is visible prior to the wire excitation, since the scraper in the parking position already touches the beam halo.

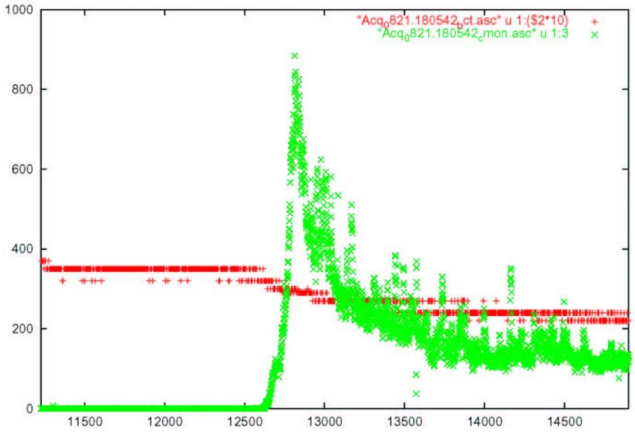

Figure 30: Beam current (BCT) and beam-loss signal (PMT) versus time in ms, for a wire excitation of 267 A starting at 12725 ms.

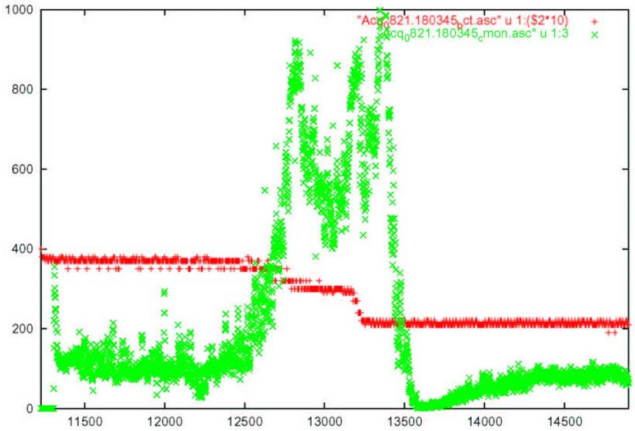

Figure 31: Beam current (BCT) and beam-loss signal (PMT) versus time in ms, for a wire excitation of 267 A starting at 12725 ms followed by mechanical scraping at 13325 ms.

4. EXTENSION OF SPS EXPERIMENT

The goal of our experiment is to demonstrate the correction of the long-range beam-beam effect in the LHC. To achieve this, two further devices will be installed in the SPS for the 2004 run, and each of these can be used to compensate the effect of the present wire. For one of the two new wires, the difference in betatron phase to the present device will be 2 degrees, about the same value as the expected average phase difference between the proposed wire and the parasitic collisions in the LHC. The new devices are each equipped with three wires, in the two transverse planes and at 45 degrees. The wires are mobile, as we aim to move the compensating wire 2-3σ further out than the perturbing primary wire and to observe the consequences. Also the impact of excitation strength errors of order 10% will be studied in the next series of SPS experiments. The second new wire device will explore the compensation over a long distance, with a variable betatron-phase advance and with the possibility of independent horizontal and vertical orbit bumps. This third wire will confirm the practicability of the proposed wire compensation for the LHC with reduced systematic cancellations and it will explore realistic tolerances. Finally, an additional application of the new devices is to compare the effects of alternating x-y crossings at two IPs (LHC baseline) with a two times stronger collision at 45 degree (inclined hybrid crossing) and with pure vertical or pure horizontal crossings. This will probe the sensitivity to the LHC crossing scheme and assess the present choice.

5. SUMMARY AND OUTLOOK

The long-range beam-beam compensator prototype that is installed in the SPS models the effect of long-range collisions in the Large Hadron Collider. This prototype consists of a water-cooled wire in the vacuum chamber, mounted parallel to the beam at a distance of several rms beam sizes, through which a current of up to 300 A can be fed. So far 3 machine experiments were performed in 2002 and 3 further in 2003. The tune shift and closed-orbit orbit distortions are well understood and they both allow for a precise determination of the beam-wire distance to within a few percent. The measurements of beam lifetime and beam loss indicate that the LHC design parameters are close to an edge, i.e., for a 10% smaller crossing angle, the beam lifetime might drop to 4 h. We observed a distinct shrinkage of the beam emittance due to particle loss at large amplitudes, when the wire is excited, and we studied its dependence on the wire current and on the beam-wire separation. The wire scans used for emittance measurements were calibrated by mechanical scraping at a known amplitude. Using this calibration, we were able to deduce an effective dynamic aperture from the wire scans performed with wire excitation. This dynamic aperture varies linearly with the square root of the excitation current, which confirms a scaling law predicted many years ago by J. Irwin [1]. As a result, we obtain a lower bound on the LHC dynamic aperture of 2σ. We suspect that this lower bound is an artefact of the limited physical aperture in the SPS at 26 GeV/c, where the measurement was executed. Attempts to directly measure amplitude-dependent diffusion rates by recording photo-multiplier signals after fast scraper retraction have so far proven difficult, due to a great variation of the signals from different photomultipliers, the limited scraper speed, and, through 2003, a restricted flexibility in the application software. More work is needed to quantitatively ascertain the threshold for the onset of chaos and the extrapolation to the LHC. We foresee further experiments, e.g., with an upgraded scraper software, and also additional analysis, e.g., by exploiting 1000-turn data recorded by the beam-position monitors after 'kicking' the beam. Two more devices will become available in 2004. These will demonstrate the correction efficiency and its sensitivity to errors and, each being equipped with several wire at different transverse positions, they will also allow a comparison of various crossing schemes, e.g., horizontal-vertical crossing at two interaction points, pure horizontal-horizontal crossing, or crossings at 45 degrees.

Acknowledgements

We wish to thank all the many colleagues and groups who made this experiment possible, in particular G.Burtin, J. Camas, G. Ferioli, S. Myers, G. de Rijk, M. Royer, and H. Schmickler.

References

[1] J. Irwin, "Diffusive Losses from SSC Particle Bunches due to Long-Range Beam-Beam Interactions," SSC-233 (1989).

[2] D. Neuffer, S. Peggs, "Beam-Beam Tune Shifts and Spreads in the SSC: Head-On, Long Range and PACMAN conditions," SSC-63 (1986).

[3] W. Herr, "Tune Shifts and Spreads due to the Long-Range Beam-Beam Effects in the LHC," CERN/SL/90-06 (AP) (1990).

[4] T. Sen, et al., "Effect of the beam-Beam Interaction on the Dynamic Aperture and Amplitude Growth in the LHC," Beam-Beam Effects in Large Hadron Colliders LHC99, CERN-SL-99-039 AP (1999).
[5] Y. Papaphilippou, F. Zimmermann, "Weak-Strong Beam-Beam Simulations for the Large Hadron Colliders," PRST-AB 2:104001 (1999).
[6] H. Grote, P. Leunissen, F. Schmidt, "LHC Dynamic Aperture at Collision," CERN LHC Project Note 197 (1999).
[7] R. Assmann, F. Schmidt, et al., "Equilibrium Beam Distribution and Halo in the LHC," Proc. EPAC2002 Paris (2002).
[8] J.-P. Koutchouk, "Principle of a Correction of the Long-Range Beam-Beam Effect in the LHC Using Electromagnetic Lenses," CERN-LHC-Project-Note 223 (2000).
[9] J.-P. Koutchouk, "Correction of the Long-Range Beam-Beam Effect in LHC using Electromagnetic Lenses," Proc. PAC2001, Chicago, p. 1681 (2001).
[10] F. Zimmermann, "Weak-Strong Simulation Studies for the LHC Long-Range Beam-Beam Compensation," Proc. Beam-Beam Effects in Circular Colliders, Fermilab (ed. T. Sen and M. Xiao), June 2001 and in CERN-LHC-Project-Report-502 (2001).
[11] P.W. Krempl, "The Abel-type Integral Transformation with the Kernel $(t^2-x^2)^{-1/2}$ and ite Application to Density Distributions of Particle Beams," CERN Note MPS/Int. BR/74-1 (1974).
[12] C. Carli, A. Jansson, M. Lindroos, H. Schonauer, "A Comparative Study of Profile and Scraping Methods for Emittance Measurements in the PS Booster, CERN-PS-2000-062-OP.
[13] L. Michelotti, "Integral for Longitudinal Phase Space Tomography on Equilibrium Distributions," PRST-AB 6, 024001 (2003).
[14] M. Seidel, "The Proton Collimation System of HERA," Ph.D. Thesis, DESY-94-103 (1994).